Journal of Applied Mechanics and Technical Physics, Vol. 44, No. 1, pp. 64–68, 2003

ORIGINATION OF IN-PHASE OSCILLATIONS OF THIN PLATES WITH AEROELASTIC INTERACTION

A. L. Tukmakov

UDC 533.6.013.42

Synchronization of oscillations of thin elastic plates that are walls of a gas-filled channel is considered. The gas motion is described by a system of Navier–Stokes equations, which is solved using the second-order MacCormack method with time splitting. The motion of the channel walls is described by a system of geometrically nonlinear dynamic equations of the theory of this plates, which is solved by the finite-difference method. Kinematic and dynamic contact conditions are imposed at the interface between the media. A numerical experiment is performed to determine typical dynamic regimes and study the transition of the aeroelastic system to in-phase oscillations.

Key words*: gas motion, oscillations of an elastic plate, splitting method.*

The mutual effect of elements that compose a spatially coupled nonlinear system leads sometimes to synchronization of oscillations of these elements [1, 2]. This phenomenon is observed in chemical reactions, coupled generators, in oscillations of pendula of clocks on a common base, etc. In the present work, methods of mathematical simulation are used to study synchronization of the phases of oscillations of elastic plates, which are sectors of the upper and lower walls of a plane channel filled by air. Processes that occur in the gas and accompany synchronization of the phases of oscillations of these plates for various parameters of external excitation are considered.

1. Model and System of Equations. We considered a plane channel filled by a gas. The upper and lower walls of this channel are elastic within $-l \leqslant x \leqslant l$ and rigid outside this interval (Fig. 1). Under asymmetric excitation of oscillations of elastic walls by single pulses of external pressure, aeroelastic oscillations with different amplitudes and phases are first observed. After a certain time, synchronization of oscillations of the channel walls occurs due to their mutual influence through the gas medium.

To describe the gas motion in the channel, we used the Navier–Stokes equations for a compressible heat-conducting gas [3], written in the Cartesian coordinate system:

$$\boldsymbol{q}_t + \boldsymbol{F}_x + \boldsymbol{G}_y = 0. \tag{1}$$

Here

$$\boldsymbol{q} = \begin{bmatrix} \rho \\ \rho u \\ \rho v \\ E \end{bmatrix}, \quad \boldsymbol{F} = \begin{bmatrix} \rho u \\ \rho u^2 + p - \tau_{xx} \\ \rho uv - \tau_{xy} \\ (E + p - \tau_{xx})u - \tau_{xy}v + Q_x \end{bmatrix}, \quad \boldsymbol{G} = \begin{bmatrix} \rho v \\ \rho uv - \tau_{xy} \\ \rho v^2 + p - \tau_{yy} \\ (E + p - \tau_{yy})v - \tau_{xy}u + Q_y \end{bmatrix},$$

$$Q_x = -k\,\frac{\partial T}{\partial x}, \quad Q_y = -k\,\frac{\partial T}{\partial y}, \quad p = (\gamma - 1)\Big(E - \rho\,\frac{u^2 + v^2}{2}\Big),$$

$$\tau_{xx} = \mu\Big(2\,\frac{\partial u}{\partial x} - \frac{2}{3}\,D\Big), \quad \tau_{yy} = \mu\Big(2\,\frac{\partial v}{\partial y} - \frac{2}{3}\,D\Big), \quad \tau_{xy} = \mu\Big(\frac{\partial u}{\partial y} + \frac{\partial v}{\partial x}\Big), \quad D = \frac{\partial u}{\partial x} + \frac{\partial v}{\partial y}.$$

Institute of Mechanics and Mechanical Engineering, Kazan' Research Center, Kazan' 420111. Translated from Prikladnaya Mekhanika i Tekhnicheskaya Fizika, Vol. 44, No. 1, pp. 77–82, January–February, 2003. Original article submitted May 24, 2002.

 0021-8944/03/4401-0064 $25.00

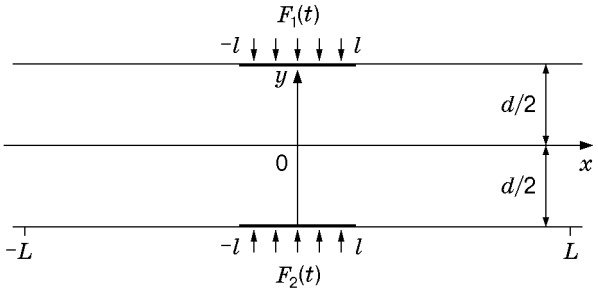

Fig. 1. Schematic of the channel.

In the domain with varied boundaries, system (1) is written in the time-dependent generic coordinates [4] $\xi = \xi(x, y, t)$, $\eta = \eta(x, y, t)$, and $\tau = t$:

$$\boldsymbol{q}_t^* + \boldsymbol{F}_\xi^* + \boldsymbol{G}_\eta^* = 0.$$

Here

$$\boldsymbol{F}^* = \frac{1}{J}\begin{bmatrix} \xi_t\rho + \xi_x\rho u + \xi_y\rho v \\ \xi_t\rho u + \xi_x(\rho u^2 + p - \tau_{xx}) + \xi_y(\rho uv - \tau_{xy}) \\ \xi_t\rho v + \xi_x(\rho uv - \tau_{xy}) + \xi_y(\rho v^2 + p - \tau_{yy}) \\ \xi_t E + \xi_x((E + p - \tau_{xx})u - \tau_{xy}v + Q_x) + \xi_y((E + p - \tau_{yy})v - \tau_{xy}u + Q_y) \end{bmatrix},$$

$$\boldsymbol{G}^* = \frac{1}{J}\begin{bmatrix} \eta_t\rho + \eta_x\rho u + \eta_y\rho v \\ \eta_t\rho u + \eta_x(\rho u^2 + p - \tau_{xx}) + \eta_y(\rho uv - \tau_{xy}) \\ \eta_t\rho v + \eta_x(\rho uv - \tau_{xy}) + \eta_y(\rho v^2 + p - \tau_{yy}) \\ \eta_t E + \eta_x((E + p - \tau_{xx})u - \tau_{xy}v + Q_x) + \eta_y((E + p - \tau_{yy})v - \tau_{xy}u + Q_y) \end{bmatrix},$$

$$\boldsymbol{q}^* = \frac{1}{J}\begin{bmatrix} \rho \\ \rho u \\ \rho v \\ E \end{bmatrix}, \quad J = \begin{vmatrix} \xi_x & \xi_y & \xi_t \\ \eta_x & \eta_y & \eta_t \\ 0 & 0 & 1 \end{vmatrix}, \quad \xi_t = -x_t\xi_x - y_t\xi_y, \quad \eta_t = -x_t\eta_x - y_t\eta_y.$$

This system was solved using the second-order explicit MacCormack method with time splitting [3, 5]. On a uniform grid, the scheme contained predictor and corrector steps whose execution allowed one to pass to the next time layer:

$$\boldsymbol{q}_{j,k}^0 = \boldsymbol{q}_{j,k}^n - \frac{\Delta t}{\Delta\xi}\Big(\boldsymbol{F}_{j+1,k}^n - \boldsymbol{F}_{j,k}^n\Big) - \frac{\Delta t}{\Delta\eta}\Big(\boldsymbol{G}_{j,k+1}^n - \boldsymbol{G}_{j,k}^n\Big),$$

$$\boldsymbol{q}_{j,k}^{n+1} = \frac{\boldsymbol{q}_{j,k}^n + \boldsymbol{q}_{j,k}^0}{2} - \frac{1}{2}\frac{\Delta t}{\Delta\xi}\Big(\boldsymbol{F}_{j,k}^0 - \boldsymbol{F}_{j-1,k}^0\Big) - \frac{1}{2}\frac{\Delta t}{\Delta\eta}\Big(\boldsymbol{G}_{j,k}^0 - \boldsymbol{G}_{j,k-1}^0\Big).$$

At the predictor and corrector steps, the derivatives with respect to ξ entering into the quantities $\boldsymbol{F}_{j+1,k}^n$ and $\boldsymbol{F}_{j,k}^n$ were replaced by the first-order left and right differences, respectively; the derivatives with respect to η were replaced by the second-order central differences. The derivatives with respect to η entering into the quantities $\boldsymbol{G}_{j,k+1}^n$ and $\boldsymbol{G}_{j,k}^n$ were approximated by the first-order left differences, and the derivatives with respect to ξ were approximated by the central differences.

The x step of the finite-difference grid in the physical domain (x, y) was constant. In the near-wall regions $-d/2 \leqslant y \leqslant -rd/2$ and $rd/2 \leqslant y \leqslant d/2$ (d is the channel height and r is a parameter defining the boundaries of the near-wall regions), cells with a fixed refined step Δy_1 were formed. In the central region $-rd/2 < y < rd/2$, cells with a larger step Δy were formed. The region (ξ, η) was a unit square with uniform partition along both axes.

The splitting scheme for the central region $-rd/2 < y < rd/2$ was a sequence of symmetric one-dimensional operators

$$\boldsymbol{q}_{j,k}^{n+1} = P_\xi(\Delta t/2)P_\eta(\Delta t/2)P_\eta(\Delta t/2)P_\xi(\Delta t/2)\boldsymbol{q}_{j,k}^n.$$

Each one-dimensional operator included the predictor and corrector steps. For instance, the action of the operator $P_\xi(\Delta t/2)$ on the vector-column $\boldsymbol{q}_{j,k}^n$ resulted in the transition to the intermediate value of $\bar{\boldsymbol{q}}_{j,k}$ in two steps:

$$\boldsymbol{q}_{j,k}^0 = \boldsymbol{q}_{j,k}^n - \frac{\Delta t}{\Delta\xi}(\boldsymbol{F}_{j+1,k}^n - \boldsymbol{F}_{j,k}^n), \quad \bar{\boldsymbol{q}}_{j,k} = \frac{\boldsymbol{q}_{j,k}^n + \boldsymbol{q}_{j,k}^0}{2} - \frac{\Delta t}{4\Delta\xi}(\boldsymbol{F}_{j,k}^0 - \boldsymbol{F}_{j-1,k}^0).$$

In regions of grid condensation, the splitting scheme included $2n$ one-dimensional operators P_η:

$$\boldsymbol{q}_{j,k}^{n+1} = P_\xi(\Delta t/2)P_\eta(\Delta t/(2n))\cdots P_\eta(\Delta t/(2n))P_\xi(\Delta t/2)\boldsymbol{q}_{j,k}^{n}$$

($n = \Delta y/\Delta y_1$).

To describe the motion of elastic sectors of the walls, we used the system of geometrically nonlinear dynamic equations of the theory of thin plates, which were obtained on the basis of the Kirchhoff–Love hypothesis [6]:

$$\begin{gathered}\frac{\partial^2 V}{\partial t^2} = \frac{E}{\rho_n(1-\nu^2)}\,\frac{\partial^2 V}{\partial x^2} + \frac{E}{\rho_n(1-\nu^2)}\,\frac{\partial W}{\partial x}\,\frac{\partial^2 W}{\partial x^2} + \frac{Z_\tau}{\rho_n},\\ \frac{\partial^2 W}{\partial t^2} = -\frac{D}{\rho_n}\,\frac{\partial^4 W}{\partial x^4} - \alpha\,\frac{\partial W}{\partial t} + \frac{Eh}{\rho_n(1-\nu^2)}\Big(\frac{\partial V}{\partial x} + \frac{1}{2}\Big(\frac{\partial W}{\partial x}\Big)^2\Big)\frac{\partial^2 W}{\partial x^2} + \frac{Z_n}{\rho_n}.\end{gathered} \tag{2}$$

Here Z_τ and Z_n are the tangential and normal components of the dynamic load, W and V are the flexure and tangential displacement of fixed (Lagrangian) points of the median surface, h and ρ_n are the thickness and density of the plate material, E is the elasticity modulus, and ν is Poisson's ratio. Structural damping was taken into account by the term $\alpha(\partial W/\partial t)$. Anchorage conditions were imposed on the longitudinal edges of the plates (Fig. 1):

$$W = 0, \quad V = 0, \quad \frac{\partial W}{\partial x} = 0 \qquad \text{for} \quad x = \pm l. \tag{3}$$

At the initial time, the plates were motionless:

$$W = 0, \quad V = 0, \quad \frac{\partial W}{\partial t} = 0, \quad \frac{\partial V}{\partial t} = 0 \qquad \text{for} \quad t = 0,\ -l \leqslant x \leqslant l. \tag{4}$$

The tangential component of the load was assumed to be zero, and the normal component contained the rigid and follow-up parts. The follow-up character was determined by the excess pressure on the elastic surface. The rigid component of loading was defined by an external pulsed excitation $F(t)$ uniformly distributed over the plate surface, and this component was independent of the plate-surface shape:

$$Z_n = F(t) + p_0 - p, \quad Z_\tau = 0, \quad F(t) = At \quad \text{for} \quad t < t_{\text{in}}, \qquad F(t) = 0 \quad \text{for} \quad t \geqslant t_{\text{in}}. \tag{5}$$

Here p and p_0 are the current and undisturbed pressure of the gas at the times t and $t = 0$ and t_{in} is the time of increasing of the external load pulse. System (2) with conditions (3)–(5) was solved by the finite-difference method using second-order implicit difference schemes [7].

The change in the shape of elastic elements altered the computational domain geometry. The finite-difference grid in the "physical" variables x and y and its mapping onto a motionless finite-difference grid in the variables ξ and η were reconstructed at each time step. The reconstruction parameters ξ_x, ξ_y, η_x, η_y, x_t, y_t, ξ_t, and η_t entering into the system of equations of gas motion, which was written in generic moving coordinates [3, 4], were determined, and the transition to the next time layer was performed using the MacCormack scheme.

Kinematic and dynamic contact conditions were set at the interface between the media. No-slip conditions were imposed on the solid surfaces for gas-velocity components: at points on the plate surface, they were assumed to be equal to the corresponding components of the plate velocity. Uniform boundary conditions of the second kind were set at all boundaries of the computational domain for density, energy, and temperature. The temperature, density, and velocity of the gas were determined in internal nodes at the initial time.

The gas-dynamic part of the software package was tested by comparing the results of numerical simulation with available experimental data [8]. The method used to model the dynamics of the elastic element was considered in [9].

The numerical experiment included simulation of aeroelastic oscillations arising under loading of elastic walls of the channel by single triangular pressure pulses whose duration was equal to half of the period of eigenoscillations of the plates at the lower resonant frequency. The channel length was chosen such that the disturbances did not reach the input and output boundaries within the time interval examined. The calculations for a channel of height $d = 0.03$ m were performed for the following values of plate parameters: thickness $h = 0.001$ m, length $2l = 0.2$ m, elasticity modulus $E = 10^{11}$ N/m^2, Poisson's ratio $\nu = 0.3$, and density $\rho_n = 4500$ kg/m^3. The number of nodes of the finite-difference grid in solving the elastic problem was $N = 60$. The following characteristics were used for the gas (air) filling the channel: ratio of specific heats $\gamma = 1.4$, universal gas constant $R = 278$ J/(kg$\cdot$K), initial temperature of the undisturbed gas $T_0 = 290$ K, and initial density $\rho_0 = 1.2$ kg/m^3. The results were obtained on a computational grid with parameters $N_j = 297$, $N_k = 40$, $N_1 = 10$, and $r = 0.8$ (N_1 is the number of nodes in the central region $-rd \leqslant y \leqslant rd$). The time step in the computations was $\Delta t = 3 \cdot 10^{-8}$ sec.

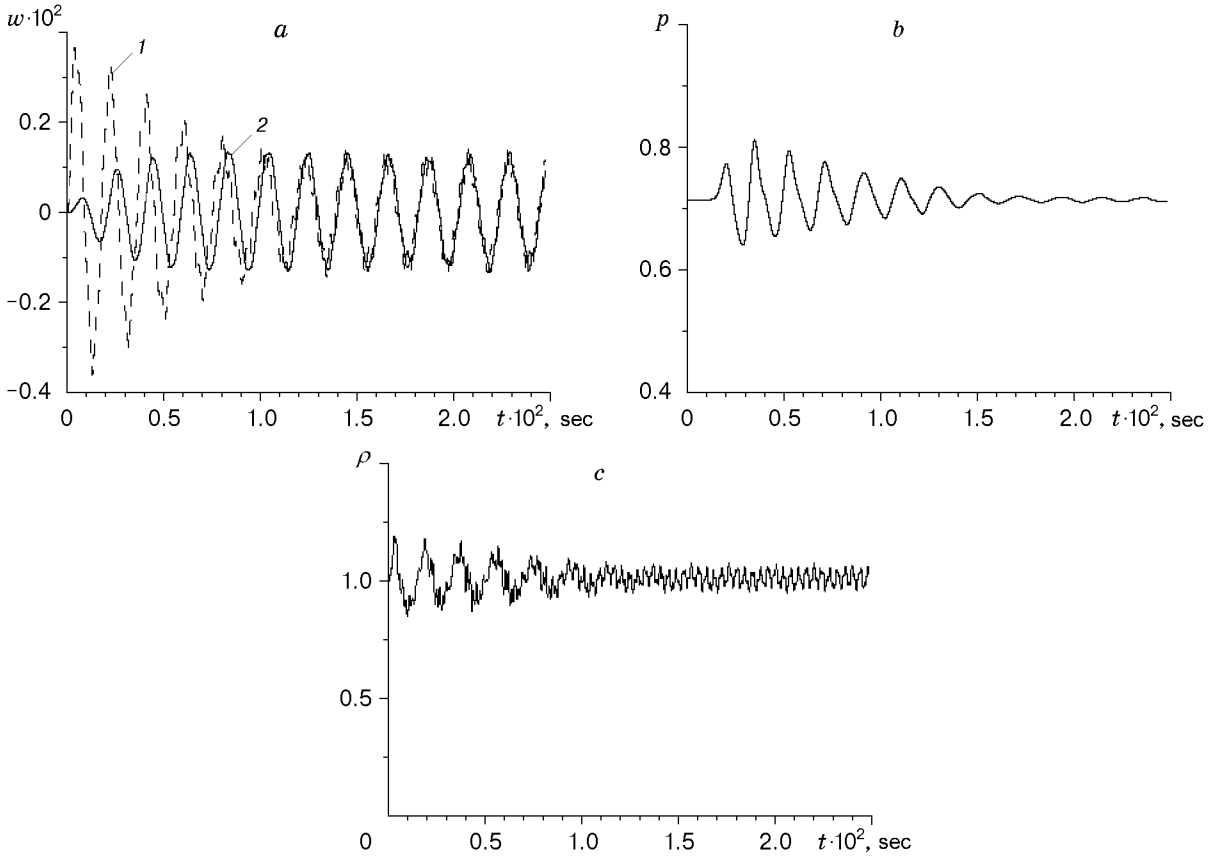

Fig. 2. Flexure of the plates (a), pressure on the channel axis for $x = -0.1$ m (b), and gas density on the channel axis for $x = 0$ (c) versus time: curves 1 and 2 show the amplitudes of oscillations of the plate with an applied external pressure pulse and the initially motionless plate, respectively.

2. Calculation Results. If the plates have identical parameters, then the dynamics of the aeroelastic system and the process of synchronization are determined by characteristics of external exciting pulses $F_1(t)$ and $F_2(t)$ acting on the elastic walls of the channel.

We consider a dynamic process arising under excitation of only one plate: $F_1(t) = At$ $(t < t_{\text{in}})$ or $F_1(t) = 0$ $(t > t_{\text{in}})$ and $F_2(t) = 0$. Figure 2a shows the flexure of the plates in time. The amplitude of oscillations of the plate to which an external pressure pulse was applied decreases with time (the energy of oscillations of this plate is spent on swinging the second plate and irradiating waves in the gas propagating along the channel). The increase in the amplitude of oscillations of the initially motionless plate is accompanied by a decrease in the phase shift. At the end of the first half-period, the phase shift of oscillations of the plates is $\pi/2$, but the phase difference of oscillations decreases with time, and oscillations are synchronized both in terms of amplitude and phase at $t > 0.01$ sec (Fig. 2a). Synchronization of motion of elastic elements is accompanied by a drastic decrease in the amplitude of oscillations of gas pressure and density in the channel. Figure 2b shows the pressure versus time at the channel axis at a point with a coordinate $x = -0.1$ m. Prior to the in-phase mode, plate oscillations are accompanied by significant changes in the channel volume bounded by elastic walls, which leads to emergence of pressure oscillations with steep leading fronts. Simultaneous displacements of the walls correspond to small changes in the channel volume; as a result, pressure oscillations have a small amplitude and are close to harmonic in shape (Fig. 2b). Figure 2c shows the density versus time at the channel axis at a point with a coordinate $x = 0$. Prior to excitation of in-phase oscillations, the signal contains the excitation frequency (frequency of oscillating plates) and frequencies multiple to the frequency of the first linear acoustic resonance of the gas column in the transverse direction f_{11} and $2f_{11}$ [8]; after synchronization, the spectral composition of the acoustic signal becomes different: the amplitude of the component with the excitation frequency drastically decreases, despite the significant amplitude of oscillations of the channel walls (Fig. 2a and c).

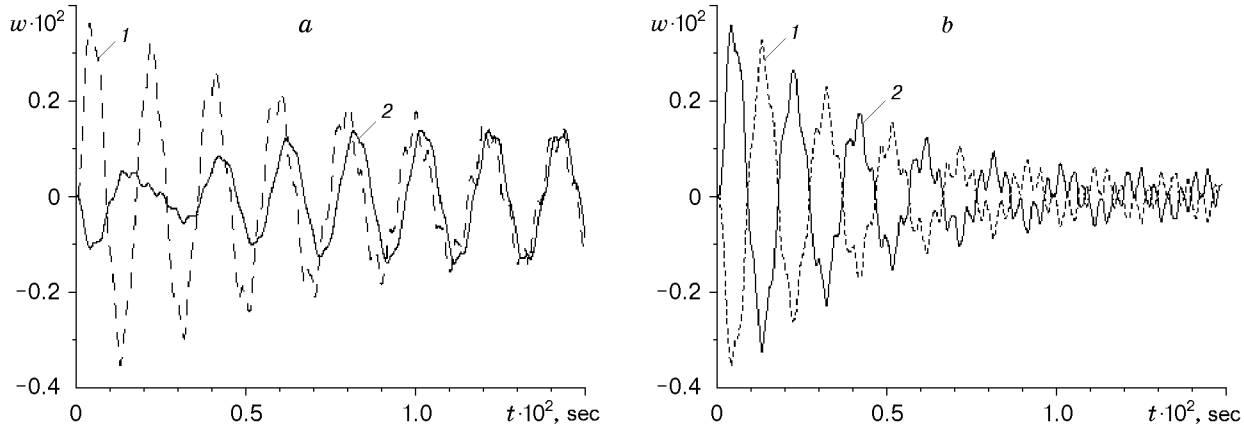

Fig. 3. Flexure of the plates versus time for $F_1(t) = At$ $(t < t_{\text{in}})$ or $F_1(t) = 0$ $(t > t_{\text{in}})$ and $F_2(t) = -0.3F_1(t)$ (a) and $-0.99F_1(t)$ (b); curves 1 and 2 show the amplitudes of oscillations of the plate with an applied external pressure pulse and the initially motionless plate, respectively.

Another type of joint oscillations is observed if the initial excitation of the plates occurs in antiphase with significantly different intensities of external pressure pulses. Figure 3a shows the flexure of the plates as a function of time for $F_1(t) = At$ $(t < t_{\text{in}})$ or $F_1(t) = 0$ $(t > t_{\text{in}})$ and $F_2(t) = -0.3F_1(t)$. The process of synchronization of amplitudes and phases occurs due to the increased duration of the period of oscillations of the plate to which the pulse of lower intensity is applied. After synchronization, the amplitude of oscillations of the plates is higher than that in the case of excitation of oscillations of one plate only. For $F_2(t) = -0.9F_1(t)$, the process of synchronization of oscillations occurs in a similar manner.

If the initial excitation of the plates occurs in antiphase with close intensities of external pressure pulses, no in-phase oscillations arise in the system. Figure 3b shows the flexure of the plates as a function of time for $F_1(t) = At$ $(t < t_{\text{in}})$ or $F_1(t) = 0$ $(t > t_{\text{in}})$ and $F_2(t) = -0.99F_1(t)$. Intense damping of oscillations of the elastic walls is observed in this regime because of the fact that the pressure distribution in the gas is close to axisymmetric. The gas-pressure growth near the channel axis with the plates moving toward the internal region leads to faster damping of their amplitude. At the same time, pressure and density oscillations arising under antiphase excitation of the plates occur with a higher intensity, as compared to the in-phase mode.

Thus, numerical simulation of interaction of aeroelastic coupled plates allowed us to reveal two most typical dynamic modes. Under symmetric excitation, plate oscillations rapidly decay without any synchronization. In the case of significantly asymmetric excitation, synchronization of the phases of the oscillating plates is observed due to an increase in the period of oscillations of the plate with a lower amplitude.

This work was supported by the Foundation of Research and Development and Design Works of the Tatarstan Republic [Grant No. 05-5.3-45/2002 (F)] and by the Federal Targeted Program "Integration" (Grant No. A0012).

REFERENCES

1. H. G. Schuster, *Deterministic Chaos: An Introduction*, Physik-Verlag, Weinheim (1984).
2. P. Bergé, Y. Pomeau, and C. Vidal, *L'ordre Dams le Chaos. Vers une Approchen Determeniste de la Turbulence*, Paris, Hermann (1988).
3. C. Fletcher, *Computational Techniques for Fluid Dynamics*, Springer-Verlag, Heidelberg (1988).
4. J. L. Steger, "Implicit finite-difference simulation of flow about arbitrary two-dimensional geometries," *AIAA J.*, **16**, No. 7, 679–686 (1978).
5. V. M. Kovenya, G. A. Tarnavskii, and S. G. Chernyi, *Application of the Splitting Method in Aerodynamic Problems* [in Russian], Nauka, Novosibirsk (1990).
6. A. S. Vol'mir, *Flexible Plates and Shells* [in Russian], Gostekhteoretizdat, Moscow (1956).
7. A. S. Vol'mir, *Shells in Liquid and Gas Flows. Problem of Aeroelasticity* [in Russian], Nauka, Moscow (1976).
8. A. L. Tukmakov and R. G. Zaripov, "Numerical simulation of subharmonic oscillations of a gas in a closed tube," *Izv. Vyssh. Uchebn. Zaved., Aviats. Tekh.*, No. 1, 64–67 (2001).
9. A. L. Tukmakov, "Nonlinear vibration model of an elastic panel under periodic loading," *J. Appl. Mech. Tech. Phys.*, **41**, No. 1, 186–191 (2000).